Measurements of asymmetries of pion single charge exchange on polarized ^{3}He at 200 MeV

Q. Zhao,* G. Burleson, S. Blanchard, T. Chang, W. Gibbs, J. Haas,† B. Park,‡ and M. Whitton§
Department of Physics, New Mexico State University, Las Cruces, New Mexico 88003

M. Espy,‡ D. Dehnhard, B. Larson, J. O'Donnell,‡ and M. Palarczyk‖
School of Physics and Astronomy, University of Minnesota, Minneapolis, Minnesota 55455

W. Cummings,¶ P. Delheij, and O. Häusser**
Tri-University Meson Facility, Vancouver, Canada V6T 2A3

E. Pasyuk and M. Gostkin
JINR, Dubna, Moscow, Russia

J. Amann, R. Boudrie, C. Riedel,†† C. Morris, S. Pentillä, D. Swenson,‡‡ and D. Tupa
Los Alamos National Laboratory, Los Alamos, New Mexico 87545

J. Comfort and C. Gaulard§§
Department of Physics, Arizona State University, Tempe, Arizona 85281

K. Maeda
Department of Physics, Tohoku University, Kawauchi, Sendai, Japan

G. Glass‡
University of Texas, Austin, Texas 78712

I. Supek
Rudjer Bošković Institute, Zagreb, Croatia

(Received 8 March 1999; published 25 June 1999)

Asymmetries for the (π^-,π^0) reaction on polarized ^{3}He were measured using a 200-MeV pion beam at LAMPF. The π^0's were detected with the neutral meson spectrometer in coincidence with the recoiling tritons. A recoil triton detector, consisting of scintillation-counter telescopes and a wire chamber, was used to measure the time-of-flight, energy loss, and direction of the tritons. The polarized gaseous ^{3}He target, developed at TRIUMF, was modified to run with two diode lasers; the polarization reached 65%. The asymmetries between $\theta_{\rm lab}=60°$ and 105° were found to be strongly angle dependent. The results are compared with theoretical calculations. [S0556-2813(99)02208-6]

PACS number(s): 24.70.+s, 25.80.Gn, 25.10.+s

I. INTRODUCTION

This experiment is part of a series of measurements of the asymmetries A_y of pion scattering from polarized ^{3}He in the energy region of the $\Delta(1232)$ resonance. Earlier measurements of A_y include $\pi^\pm$ elastic scattering at 100 MeV carried out at TRIUMF [1,2]. At LAMPF, asymmetry data were taken for π^+ elastic scattering at 142, 180, and 256 MeV [3,4], and for π^- elastic scattering at 180 MeV [4]. Here we report on the results of measurements of A_y for the (π^-,π^0) single charge exchange reaction on polarized ^{3}He at 200 MeV.

The original motivation for these measurements came from the results of experiments involving pion scattering

*Present address: University of Michigan, Ann Arbor, MI 48109.
†Present address: Allied Signal, NASA White Sands Test Facility, Las Cruces, NM 88004.
‡Present address: Los Alamos National Laboratory, Los Alamos, NM 87545.
§Present address: National High Magnetic Field Laboratory, Florida State University, Talahassee, FL 32310.
‖Present address: Ohio University, Athens, OH 45701. Permanent address: Henryk Niewodniczański Institute of Nuclear Physics, 31-342 Kraków, Poland.
¶Present address: Argonne National Laboratory, Argonne, IL 60439.
**Deceased.
††Present address: University of Montana, Missoula, MT 59812.
‡‡Present address: Varian Ion Implant Systems, Gloucester, MA 01930.
§§Present address: Lab. Nazionali di Frascati dell'INFN, Frascati, Italy.

from polarized ^{15}N [5,6] and ^{13}C [7–10], both nuclei with spin and isospin 1/2. Whereas the experiments found small A_y, theory [11,12] predicts large values. The failure of theoretical calculations to reproduce the experimental A_y indicates that either the π-nucleus reaction mechanism is not adequately understood, or that the nuclear wave functions of ^{13}C and ^{15}N are not sufficiently well known, or both. Therefore it was decided to conduct A_y measurements on a nucleus with well-understood nuclear structure, such as ^{3}He.

^{3}He is one of the simplest nuclei with spin and isospin 1/2. Reliable ^{3}He wave functions have been derived by Faddeev calculations [13–15]. Its ground state contains S, S', and D components. The predominate one is the S state ($\sim$90%) with the spin-up and the spin-down proton coupled to spin zero and the neutron carrying the nuclear spin. In the S' state ($\sim$2%), the proton and neutron couple to form a quasideuteron, with the other proton having a spin in the opposite direction. In the D state ($\sim$9%), all the nucleons (protons and neutron) have the same spin direction, oriented opposite to the ^{3}He orbital angular momentum $L=2$.

The experiments with polarized ^{3}He were possible because of the development at TRIUMF of high-density gaseous polarized ^{3}He targets that employ optical pumping [16]. The first experiments carried out at TRIUMF with these targets at 100 MeV found large asymmetries near the cross-section minima ($\sim$70°–80°), with A_y values for π^- about half as large as those for π^+. These results were in fair agreement with theoretical calculations [2,16,17] which gave good agreement with the experimental differential cross sections.

Theory indicated little dependence on the reaction model at this energy but predicted that A_y should become increasingly sensitive to the details of the reaction model as pion energies pass through the $\Delta(1232)$ resonance [17,18]. This expectation, namely, that experiments at higher energies should give more information about the spin-dependent parts of the pion-nucleus interaction, was the principal motivation for the measurements at LAMPF.

The asymmetries for π^+ elastic scattering, measured at 142, 180, and 256 MeV [3,4], were found to differ from conventional pion-nucleus interaction predictions. In order to improve the agreement between experiment and theory, it was found necessary to include a large second-order contribution to the spin-dependent scattering amplitude for π^+-^{3}He scattering which corresponds to a Δ-neutron spin-spin interaction [3,4]. This amplitude is unimportant for elastic π^- scattering and indeed, neither experiment nor theory exhibits the large negative A_y near 60° which are characteristic for π^+ elastic scattering at Δ-resonance energies. However, the predictions of A_y for π^- were found to be a factor of two too small [4].

The experiment described here was carried out to gather further information on the spin dependence of the π-^{3}He interaction. In contrast to pion elastic scattering, in which the pion interacts with all three nucleons but the spin dependence comes principally from the interaction with the neutron, the spin dependence of the charge exchange reaction principally involves an interaction with the proton whose spin is opposite to that of the ^{3}He nucleus, as we explain below.

The experiment was performed in the P^3-West channel of LAMPF with a modified TRIUMF ^{3}He target system which used newly-developed diode-laser optical pumping. The π^0's were detected with the new neutral meson spectrometer (NMS) in coincidence with the recoil triton in a recoil triton detector (RTD). The incident pion energy was 200 MeV, near the $\Delta(1232)$ resonance.

Section II presents a theoretical description of the pion-nucleus interaction. Section III gives details of the experiment, and Sec. IV describes the data analysis. Section V presents the results and a comparison with theoretical calculations, and Sec. VI is a summary.

II. ASYMMETRY CALCULATIONS

The π-spin-$\frac{1}{2}$ nucleus interaction can be expressed in terms of the amplitude $\mathcal{F}(\mathbf{k}',\mathbf{k})=\mathcal{F}(\theta)$, where $\mathbf{k}$ and $\mathbf{k}'$ represent the initial and final momenta of the pion, respectively, in the center of mass (c.m.) frame,

$$\mathcal{F}(\theta)=f(\theta)+ih(\theta)\boldsymbol{\sigma}\cdot\mathbf{n}. \tag{1}$$

Here, $f(\theta)$ is the spin-independent amplitude, $h(\theta)$ is the spin-dependent amplitude, and $\mathbf{n}=(\mathbf{k}\times\mathbf{k}')/|\mathbf{k}\times\mathbf{k}'|$ is a unit vector normal to the scattering plane. The amplitudes, $f(\theta)$ and $g(\theta)$, can be expanded as

$$f(\theta)=\sum\ [(l+1)f_{l+}+lf_{l-}]P_l(\cos\theta) \tag{2}$$

and

$$h(\theta)=\sum\ (f_{l+}-f_{l-})P_l'(\cos\theta), \tag{3}$$

where f_{l+} and f_{l-} are the partial-wave scattering amplitudes for $j=l+\frac{1}{2}$ and $j=l-\frac{1}{2}$, respectively.

The crosssection for scattering from a 100%-polarized target can be written in terms of these amplitudes as

$$\left(\frac{d\sigma}{d\Omega}\right)_{\pm}=\langle\mathbf{k}'|[f^*(\theta)\mp ih^*(\theta)\boldsymbol{\sigma}\cdot\mathbf{n}][f(\theta)\pm ih(\theta)\boldsymbol{\sigma}\cdot\mathbf{n}]|\mathbf{k}\rangle$$

$$=|f(\theta)|^2+|h(\theta)|^2\pm\mathrm{Im}[f(\theta)h^*(\theta)]. \tag{4}$$

Here $(d\sigma/d\Omega)_+$ and $(d\sigma/d\Omega)_-$ denote cross sections for pion scattering from a target polarized parallel and antiparallel to $\mathbf{n}$, respectively. The differential cross section is given by

$$\frac{d\sigma}{d\Omega}=\frac{1}{2}\left[\left(\frac{d\sigma}{d\Omega}\right)_+ +\left(\frac{d\sigma}{d\Omega}\right)_-\right]=|f(\theta)|^2+|h(\theta)|^2,$$

and the asymmetry (or analyzing power) is given by

$$A_y=\frac{(d\sigma/d\Omega)_+-(d\sigma/d\Omega)_-}{(d\sigma/d\Omega)_++(d\sigma/d\Omega)_-}=\frac{2\,\mathrm{Im}[f(\theta)h^*(\theta)]}{|f(\theta)|^2+|h(\theta)|^2}. \tag{5}$$

The cross section for pion elastic scattering from most nuclei with spin $\frac{1}{2}$ is dominated by the spin-independent amplitude since usually $|f(\theta)|^2 \gg |h(\theta)|^2$, because all of the nucleons contribute coherently to $f(\theta)$, whereas only one nucleon (the unpaired one) contributes to $h(\theta)$. Although this effect is smaller in the three-nucleon system than in heavier nuclei, it still acts to reduce the sensitivity of the differential cross section to the spin-dependent amplitude. We see from Eq. (5) that A_y is an observable which is sensitive to the $h(\theta)$ amplitude.

The calculation of the π^--^{3}He single charge exchange reaction presented here was made with the distorted wave impulse approximation (DWIA). In this approximation the amplitude for the π^- charge exchange reaction $\mathcal{F}_{if}$ is given by

$$\mathcal{F}_{if} = \langle \chi_f^{(-)} | \langle \Psi_f | t_{\rm cx} | \Psi_i \rangle | \chi_i^{(+)} \rangle, \tag{6}$$

where $|\Psi_i\rangle$ and $|\Psi_f\rangle$ are the initial and final nuclear states, and $\chi_i^{(+)}$ and $\chi_f^{(-)}$ correspond to the distorted waves of the incoming π^- and outgoing π^0, respectively.

The pion-nucleon charge exchange operator $t_{\rm cx}$ represents (in principle) reactions taking place on both protons. However, the charge exchange can take place on only one of the protons if the ground state of ^{3}He is assumed to be a pure S state. If we choose the axis of quantization along the direction perpendicular to the scattering plane, the only spin operator active is σ^z, so that there is no spin flip (change of spin projection) for either the nucleon or the nucleus. In order for the final neutron, which corresponds to the initial proton on which charge exchange takes place, to be paired with the other (untouched) neutron to give spin zero for the pair, the charge exchange must take place on the proton with spin opposite to that of the initial ^{3}He nucleus. Hence, without any distortion of the incident and final waves, the asymmetry would be expected to be just the free charge exchange asymmetry with the opposite sign. Indeed, this is the case at the forward angles, not only for the calculations presented here, but for those of Kamalov *et al.* [17] as well, as we shall see later.

In the DWIA calculation the initial and final pion distorted wave must be calculated for use in Eq. (6). This is done by solving a truncated Klein-Gordon equation with the optical potential for the interaction of a pion with a neutron or proton in momentum space being written as [19–21]

$$V(\mathbf{q},\mathbf{q}') = [b_0 v_0(q) v_0(q') + b_1 \mathbf{q}\cdot\mathbf{q}' v_1(q) v_1(q')] \times \rho(|\mathbf{q}-\mathbf{q}'|), \tag{7}$$

where b_0 and b_1 are written (explicitly for a π^- in terms of the π-nucleon phase shifts $\delta_{2I,2J}$) as

$$b_0^{(n)} = \frac{4\pi s k^2}{m^2 k_L^3} S_{31}, \tag{8}$$

$$b_0^{(p)} = \frac{4\pi s k^2}{m^2 k_L^3} \frac{[2S_{11}+S_{31}]}{3}, \tag{9}$$

$$b_1^{(n)} = \frac{4\pi s}{m^2 k_L^2} [2P_{33}+P_{31}], \tag{10}$$

$$b_1^{(p)} = \frac{4\pi s}{m^2 k_L^2} \frac{[2P_{33}+P_{31}+4P_{13}+2P_{11}]}{3}, \tag{11}$$

where s is the square of the πN center of mass energy, m is the mass of the nucleon, and

$$S_{2I,2J}, P_{2I,2J} = \frac{e^{2i\delta_{2I,2J}}-1}{2i}. \tag{12}$$

Similar expressions hold for the final neutral pion. The pion-nucleon form factors are taken to be

$$v_{0,1} = \frac{\alpha_{0,1}^2 + k^2}{\alpha_{0,1}^2 + q^2}, \tag{13}$$

where $\alpha_{0,1} = 600$ MeV/c. Finally, $\rho(|\mathbf{q}-\mathbf{q}'|)$ is the Fourier transform of the density $\rho(r)$ of the neutron or proton, normalized to 4π.

The nonlocal potential $V(\mathbf{r},\mathbf{r}')$ is the Fourier transform of $V(\mathbf{q},\mathbf{q}')$:

$$V(\mathbf{r},\mathbf{r}') = \frac{1}{(2\pi)^6} \int d\mathbf{q} d\mathbf{q}' V(\mathbf{q},\mathbf{q}') e^{-i\mathbf{q}\cdot\mathbf{r}} e^{i\mathbf{q}'\cdot\mathbf{r}'} \tag{14}$$

$$= \sum Y_l^m(\hat{\mathbf{r}}) Y_l^m{}^*(\hat{\mathbf{r}}') V_l(r,r'). \tag{15}$$

The distorted wave function can be expanded as

$$\chi(\mathbf{k},\mathbf{r}) = 4\pi \sum_{l,m=-l}^{l} i^l Y_l^m{}^*(\hat{\mathbf{r}}) Y_l^m(\hat{\mathbf{k}}) \frac{U_l(r)}{r}, \tag{16}$$

where $U_l(r)$ is the wave function of the partial wave l obtained by solving the truncated Klein-Gordon equation

$$U_l''(r) + \frac{l(l+1)}{r^2} U_l(r) - \int_0^\infty dr' W(r,r') U_l(r') + k^2 U_l(r) + i b_2 \rho(r) U_l(r) = 0, \tag{17}$$

with

$$W(r,r') \equiv 2\omega r V_l(r,r') r'.$$

Here ω is the pion energy and b_2 is a coefficient representing the true absorption of the pion.

We take a finite-range representation of the charge exchange operator $t_{\rm cx}$ as

$$t_{\rm cx}(E,\mathbf{q},\mathbf{q}') = \lambda_0(E) v_0(q) v_0(q') + \lambda_1(E) \mathbf{q}\cdot\mathbf{q}' v_1(q) v_1(q') + \lambda_f(E) \boldsymbol{\sigma}\cdot\mathbf{q}\times\mathbf{q}' v_1(q) v_1(q'). \tag{18}$$

The complex amplitudes $\lambda_0(E)$, $\lambda_1(E)$, and $\lambda_f(E)$ correspond to the s-wave, p-wave, and spin-flip amplitudes in the pion-nucleon charge exchange, respectively. They are calcu-

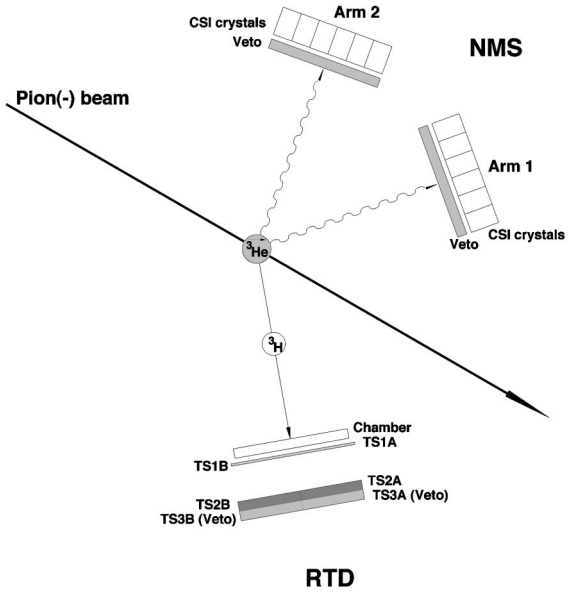

FIG. 1. Top view of the experimental setup.

lated from free pion-nucleon phase shifts. For pion kinetic energies around 200 MeV, the $l=0$ and $l=1$ partial waves are adequate to describe the pion-nucleon interaction. Parameters corresponding to an energy shift (E_{shift}), the angle transform (X_{at}), and true absorption (b_2) are treated as adjustable in the calculation. Estimates of these quantities can be made [19].

III. THE EXPERIMENT

The experiment was carried out at the Clinton P. Anderson Meson Physics Facility (LAMPF). The polarized ^{3}He target apparatus was a modified version of the high-density, optically pumped system developed at TRIUMF [1]. The neutral meson spectrometer (NMS) developed at LAMPF was used for the π^0 detection, and a recoil triton detector (RTD) was used to detect the recoiling tritons in coincidence. A sketch of the experimental setup is shown in Fig. 1.

A. The polarized ^{3}He target

A newly developed optical pumping system utilizing diode lasers was used with a version of the TRIUMF ^{3}He target system [22]. The ^{3}He gas, some nitrogen, and a small amount of rubidium were contained in a spherical glass cell of diameter 3.5 cm, made of Corning 1720 glass. The thickness of the glass wall was about 110 μm.

The ^{3}He target setup included the NMR system, Helmholtz coils that provided a holding field of variable direction, a target heating system, a diode laser, temperature control and cooling system, and a mechanical support for the target cell. The latter consisted of a VESPEL frame inside an oven surrounding the target. Since the Rb inside the target cell is solid at room temperature, it must be heated so that some of it evaporates. This was accomplished by the target heater that raised the target temperature to $\sim 170\,^\circ$C.

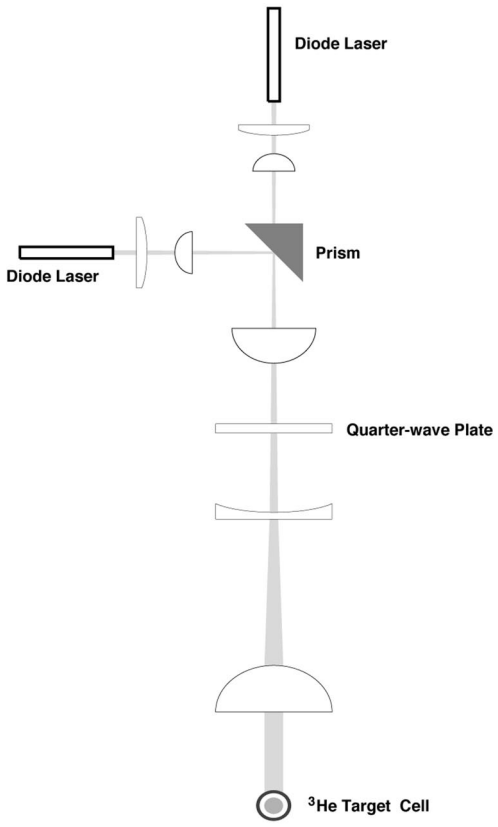

FIG. 2. Schematic diagram of the diode laser optical pumping system.

^{3}He polarization was achieved through the contact hyperfine interaction between the nuclear spin of the ^{3}He and the atomic spin of the alkali (Rb), which was polarized by the optical pumping process. At a pressure of ~ 5 atm, a volume ~ 20 cm^3 and temperature of 170 °C, the ^{3}He number density was $\sim 10^{20}$ nuclei/cm^3. The partial pressure of N_2, needed as a buffer gas, was about 100 Torr.

The diode lasers, supplied by Optopower, generated light of wave length $\lambda = 794.5$ nm for pumping the Rb atoms from the $s_{1/2}$ state to the $p_{1/2}$ state. The width of the light spectrum was $\Delta\lambda = 1.60$ nm (FWHM) which corresponds to a frequency range of $\Delta\nu = 475$ GHz (FWHM). This is much larger than the nuclear spin hyperfine splitting of 3.036 GHz for ^{85}Rb and 6.868 GHz for ^{87}Rb. The diode laser temperature and output light wavelength were controlled by a cooling system. Its temperature was adjusted to stabilize the wavelength of the laser light. Laser diodes are considerably less expensive and more reliable than the combinations of Argon and Ti:Sapphire lasers [1] that were used with the original TRIUMF target system.

A sketch of the optical system is shown in Fig. 2. Two diode lasers produced beams of linearly polarized light of 40 W total power. The two beams were focused, one of them was passed through a prism, and the other was reflected by that prism. The joint beam then went through a quarter-wave plate which changed the linear polarization of the light to circular polarization. Finally, the beam passed through a group of lenses, and a single parallel beam intersected the

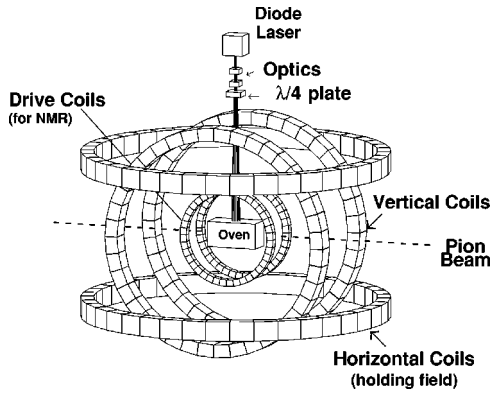

FIG. 3. The polarized ^{3}He target system.

^{3}He target cell for optical pumping.

A diagram of some of the hardware of the ^{3}He target system is presented in Fig. 3. The ^{3}He target cell was located in the center of the Helmholtz coils. There were two pairs of orthogonally oriented Helmholtz coils, one mounted with the symmetry axis oriented to provide a vertical magnetic field (about 2.4 mT) and the other mounted with the coils in the horizontal direction. Together the two sets of coils could provide a holding field in any direction.

The ^{3}He spin direction was flipped every 10 min during data acquisition. The spin flip was controlled by the adiabatic spin rotator (ASR) developed at TRIUMF [1,22]. Whenever a run was started, a subprocess for spin flip was begun in the computer. For a spin flip, the computer issued commands to trigger the CAMAC modules to operate the motor that rotated the $\lambda/4$ wave plate either clockwise or counterclockwise. At the same time, the direction of the magnetic (holding) field was being changed. The spin direction was recorded for all events.

The polarization was measured using the method described in Ref. [1], with the absolute value found by a comparison of the NMR signal induced by the ^{3}He to that from a water sample of similar geometry. It was measured every 12 h. The maximum polarization was 65%, and the average polarization during data taking was about 40%.

B. The pion beam

The pion beam was produced at the LAMPF linear accelerator, which provided a proton beam of energy up to 800 MeV and intensity up to 1 mA. The beam had a time macrostructure of 120 Hz with a typical pulse length of 500 μsec. It passed through a switchyard into area A, where secondary beams were produced. The west area of the high-energy pion channel (P^3) was used for this experiment.

A calculation with TRANSPORT (a computer program for designing a charged particle beam transport system) was carried out to design the beam optics for this experiment. An extra pair of quadrupoles was placed inside the P^3-west cave for additional focusing needs.

An ion chamber (IC), located at the end of the P^3-west beam pipe, was used to monitor the beam flux entering the target and to provide relative normalizations between spin states. Typical beam fluxes were $10^7\,\pi$/sec. An undispersed beam tune was applied, resulting in a beam spot at the target that was approximately circular, with an estimated 98% of the beam inside a diameter of about 3.5 cm, the diameter of the ^{3}He target cell. The momentum spread in the beam was 2%, or about 6 MeV/c. Effects due to the shifting of the position of the beam spot on the target with changes in the spin state were negligible.

C. Neutral meson spectrometer (NMS)

The neutral meson spectrometer (NMS) [23] is a new generation π^0 detector, designed and constructed at LAMPF to detect π^0's with good energy resolution and large acceptance. The π^0 is short-lived ($\tau = 8\times10^{-17}$ sec) and decays electromagnetically into two photons with a 98.8% branching ratio. The two decay photons are detected in coincidence in the two separate arms of the NMS (see Fig. 1).

Normally, each arm uses an array of plastic scintillators as charged-particle veto detectors, followed by three sets of 14 BGO detectors, forming three converter planes on each arm. In any of the BGO's an electromagnetic shower can be initiated by a photon from the π^0 decay. Wire chambers, located behind the BGO counters, are used to trace the shower back to the photon conversion point in the BGO crystal, for a precise determination of the angle between the directions of the two photons. Finally, two calorimeters, consisting of 60 CsI crystals each, measure most of the energies, E_1 and E_2, of the two photons that created the shower (with some energy deposited in the BGO's). The uncertainty in the measurement of E_1 and E_2 is about 6 to 8%, so that their sum would give only an inaccurate measurement of the π^0's energy.

However, from the measurement of the photon conversion points and the position of the reaction vertex (the target), the opening angle η (the angle between the two photons) can be obtained and the π^0 energy can then be calculated to higher precision than possible by calorimetry alone. In terms of two variables, the energy-sharing parameter x,

$$x = \frac{E_1 - E_2}{E_1 + E_2}, \tag{19}$$

and the opening angle η, the total energy E_{π^0} of the π^0 is given by

$$E_{\pi^0} = m_{\pi^0}\left[\frac{2}{(1-\cos\eta)(1-x^2)}\right]^{1/2}. \tag{20}$$

Thus, the π^0 energy resolution is determined by the accuracy to which x and η can be measured. By limiting the values of x to small values less than $x_{\rm cut} = 0.1$ or 0.2, the effect of the relatively poor calorimetry on the π^0 resolution can be reduced considerably. By choosing $x_{\rm cut}$ appropriately, dx (the error in the x measurement from calorimetry) can be made to contribute to dE_{π^0} (the error in the energy measurement) an amount comparable to or smaller than that from the error in the angle measurement. Therefore, a very accurate

measurement of η can give very good energy resolution. Of course, with decreasing x, the overall efficiency of the NMS decreases.

The special conditions of this experiment did not allow good energy resolution, partly because of the relatively large target size and other effects, as we explain below. In addition, the reaction yield from the gaseous ^{3}He target was so small that much was to be gained by an increase in detection efficiency at the expense of energy resolution. Thus, there was no point to use the converter planes and wire chambers which are essential for very accurate angle (and thus energy) measurement but which limit the detection efficiency to about 39% (with three converter planes on each arm). Therefore, the BGO planes and wire chambers were removed so that photon conversion occurred only in the CsI crystals with nearly 100% efficiency.

Each calorimeter is composed of a 6×10 array of pure CsI crystals, characterized by a short radiation length (1.8 cm) and a fast response (20 ns). Each CsI crystal has a cross section of 4×4 inches on the surface facing the target. The rectangular cross section increases slightly along the length of 12 inches (18 radiation lengths) to 4.2×4.2 inches (1° taper). An integral part of the crystal is a cylindrical CsI light guide of 4-in. diameter and 2.5-in. length, making the connection between the part of the crystal of rectangular cross section and the photomultiplier. The crystals are optically isolated to prevent cross talk between crystals. The conversion point was determined from the centroid of the shower that deposited energy in several CsI crystals in and around the crystal where the conversion occurred.

The energy deposited was assumed to be proportional to the pulse height obtained from the photomultiplier that was attached to the CsI crystal. Zero pulse height was assumed to correspond to zero energy (no offset). The proportionality constant between the pulse heights and the energy deposited was obtained from the energy loss of cosmic rays in the crystals and from the energy deposited from the showers created by γ's and π^0 from reactions induced by stopped π^- in hydrogen. The signals from cosmic rays served as a rough energy calibration at low energy (about 55 MeV) and to monitor changes in the gains during the experiment. The γ rays from the $p(\pi^-,\gamma)n$ reaction and the γ rays from the decay of the π^0 from the $p(\pi^-,\pi^0)n$ reaction were used for calibration at higher γ energies (up to 130 MeV). For this purpose, a 54-MeV π^- beam was slowed down in a Be degrader and in the wall of an aluminum bottle containing hydrogen gas at high pressure (129 atm) so that a good fraction of the π^- stopped in the hydrogen gas.

For stopped π^-, the (π^-,γ) and (π^-,π^0) reactions on hydrogen produce monoenergetic γ and π^0, respectively. The single γ from the $p(\pi^-,\gamma)n$ reaction calibrates the crystals in each arm individually. The two coincident γ's of total energy 137.9 MeV from the decay of the 2.9-MeV π^0 from the $p(\pi^-,\pi^0)n$ reaction deposit in several crystals of each arm an average energy of 1/2 of the total energy. The opening angle between the two NMS arms was set to 156° for the detection of the two coincident γ's.

A two-dimensional coordinate system was used for the array of 60 crystals in each crate. The coordinates of the crystal number i were given by x_i, y_i. The coordinates x_c and y_c of the conversion point of the photon in the CsI array were then obtained from the average of the positions of the crystals, weighted by the energy deposited in the crystals that contained parts of the shower:

$$x_c=\frac{\sum x_iE_i}{\sum E_i}, \quad y_c=\frac{\sum y_iE_i}{\sum E_i}. \tag{21}$$

The sum was taken only over those crystals at and in the neighborhood of the shower centroid. This region was selected with the condition that the position calculated by Eq. (21) was not changed significantly by the addition of the signal from another adjacent crystal.

The uncertainty in the position of the conversion points of the two γ rays from this method was much larger than when the BGO converters and wire chambers are used. In addition, the dimension of the target cell in the beam direction was much larger (3.5 cm) than for the more customary sheets of solid target material. Both contributed to the uncertainty in the determination of the opening angle and thus the energy resolution. Other contributions to the energy resolution were the incident beam momentum spread and the energy loss of the incident π^- in the target cell walls. Therefore, the overall π^0 energy resolution was only about 20 MeV (FWHM), as opposed to the 1-MeV design resolution of the NMS. In spite of this very poor energy resolution, it was possible to take useful asymmetry data by detecting the residual ^{3}H from the ^{3}He(π^-,π^0) reaction with a triton recoil detector (RTD) in coincidence with the NMS. (See below.)

For π^0 identification with the NMS it was required that none of the 15 charged-particle veto scintillators in either arm fired, effectively removing events in which charged particles were produced in the target and passed into the calorimeter. ADC and TDC signals from the CsI crystals in both arms were used to remove single-photon events in which, for example, one of the decay photons from a π^0 missed detection. The events that passed the veto and the coincidence test, and that were in the pion beam gate, were considered preliminary π^0 events.

Software gates for the events that passed the hardware gate and trigger were set for π^0 identification. These consisted of a gate on the total energy (the sum of the energies E_1 and E_2, deposited in the two arms), a gate on the π^0 invariant mass, and a gate on the time difference between the detection of the two photons. Since, depending on the reaction angle and desired range of excitation energies in ^{3}H (0 to about 20 MeV), the total energy of the π^0 ranged from about 150 to about 335 MeV at the incident energy of 200 MeV, a gate on the total energy was set from 150 to 355 MeV.

In terms of the four-momentum, or the total energy E_{π^0} and the three-momentum $\mathbf{p}_{\pi^0}$, the square of the π^0 invariant mass is given by

$$m_{\pi^0}^2=P_{\pi^0\mu}P_{\pi^0}^{\mu}=E_{\pi^0}^2-\mathbf{p}_{\pi^0}^2, \tag{22}$$

or equivalently by [see Eq. (20)]

$$m_{\pi^0}^2 = E_{\pi^0}^2[(1-\cos\eta)(1-x^2)/2]. \quad (23)$$

Using the energies E_1 and E_2 deposited in the CsI crystals to calculate the total energy E_{π^0} and the energy-sharing parameter x, and the positions of the target and the conversion points to determine the opening angle η, an invariant mass was calculated with Eq. (23) for all π^0 events. This resulted in an invariant mass spectrum that had a prominent peak, about 18 MeV (FWHM) wide centered at 135 MeV, the mass of the π^0. A gate of 50 MeV width was placed on this peak.

We also created a spectrum of the differences of the arrival times of the two γ's at the two arms. A time gate of 16 ns width was placed on a strong peak of width 5.7 ns (FWHM) centered at 0 ns. This gate reduced background by excluding a large fraction of coincidences between γ's from two different π^0.

D. Recoil triton detector (RTD)

The ^{3}H were detected by the recoil triton detector (RTD) that was specifically developed for this experiment (Fig. 1). The tritons were identified by energy losses, time-of-flight (TOF), and fast-particle vetoes.

The RTD consisted of four layers. The first layer was a wire chamber which recorded the recoil particle's position as it entered the RTD, which in turn gave the triton's emission angle. Layers two to four consisted of pairs of scintillation detectors (Fig. 1). The scintillators TS1A, TS1B, TS2A, and TS2B were used to measure the energy losses. TS1A and TS1B were 1.6 mm thick and recorded an energy loss ΔE. TS2A and TS2B were chosen to be 6.3 mm thick so that the tritons would definitely be stopped. They recorded the residual energy E of stopping particles or the energy loss of passing particles.

Most tritons from the charge exchange on the polarized ^{3}He would stop in TS2A or TS2B. However, due to energy straggling in the various materials between the reaction vertex and the RTD, some tritons stopped in TS1A and TS1B. The last layer of scintillators, TS3A and TS3B, were used to veto fast charged particles such as electrons, pions, protons, and deuterons that penetrated the first two layers of scintillators. The residual nuclei from the charge exchange on the Al, Si, and O in the glass walls of the target stopped either in the cell's glass or in the air (before they reached the RTD) because of their low energies.

The operation of the scintillators TS1A, TS1B, TS2A, and TS2B to detect ΔE and E of the tritons was tested using a beam of 525 MeV/c momentum, originating at the pion-production target. This beam contained a contamination of tritons, presumably from $(p,p't)$ and (p,t) reactions on the production target. It was directed at the RTD that had been placed at 0°. The kinetic energy of the tritons was 40 MeV, somewhat larger than the triton recoil energies of 32.5 MeV and 22.8 MeV, respectively, from the ^{3}He(π^-,π^0) reaction at the two angle settings of the RTD in this experiment (40° and 50°).

Note that we chose 200 MeV for the incident energy rather than 180 MeV, where the A_y for π^+ and π^- elastic scattering had been measured, because the recoil energies at 180 MeV incident energy would have been smaller and the detection of the tritons would have been more difficult. Fortunately, at 200 MeV, differential cross section data exist for the single charge exchange reaction [24,25]. No attempt was made to remeasure cross sections in the present study because of the difficulty in calculating the absolute efficiency of the NMS-RTD system to the needed accuracy. Of course, the absolute efficiency is not needed for a measurement of asymmetries.

The TDC information from TS1A and TS1B was used for additional ^{3}H identification by time-of-flight (TOF). We used a start signal from the π^0 event in the NMS and a stop signal from the RTD to create a TOF spectrum. A particle identification box was then placed on two-dimensional histograms of the energy loss in TS1A and TS1B versus the particles' TOF. The time scale of the TOF spectrum was calibrated by the reaction ^{2}H$(\pi^+,\pi^0)2p$ at an incident energy where the protons have velocities equivalent to that of the tritons from the ^{3}He$(\pi^+,\pi^0)^3$H reaction.

The RTD effectively removed background from reactions that produce a π^0 in coincidence with charged particles other than tritons. For example, the quasifree charge exchange reaction ^{3}He$(\pi^-,\pi^0;n)^2$H contributes events to the π^0 spectra starting at a missing mass of about 9 MeV, which are thus not resolved from the transition to the ground state of ^{3}H with our 20-MeV (FWHM) resolution. The veto scintillators and the coincidence requirement with a recoiling (bound) triton eliminated many π^0 that were correlated with the deuterons from the triton continuum.

However, there were tritons in coincidence with π^0 from three-body reactions on the nuclei in the target cell glass which had to be eliminated as much as possible. Whereas the particles from the two-body final state of the ^{3}He$(\pi^-,\pi^0)^3$H reaction are coplanar, only relatively few correlated π^0-triton pairs from a three-body reaction are coplanar. Thus, we used the triton angles obtained from the RTD wire chamber to reduce the number of background tritons (and other particles) from reactions such as ^{28}Si$(\pi^-,\pi^0t)^{25}$Mg. For this purpose, we extracted the azimuthal angle of both the π^0 from the NMS (ϕ_{π^0}) and the recoil particle from the RTD wire chamber (ϕ_{RTD}). A software gate placed on the difference $\Delta\phi = |\phi_{\pi^0} - \phi_{\mathrm{RTD}}|$ around the value of 180° expected for a two-body final state reduced the background from three-body reactions on the glass. The gates were set at ± 100 mrad, around a peak of width 102 mrad (FWHM) centered at 0 mrad.

E. Empty-target measurements and final spectra

Figure 4 shows the π^0 missing mass spectra after software cuts for π^0 identification in the NMS, ^{3}H identification in the RTD, and kinematic coincidence between the π^0 and the triton. Although much of the background was eliminated by these cuts and the coincidence requirement, there was still a lot of background present in the spectra, mostly from reactions on the cell glass. For this reason, data were taken with

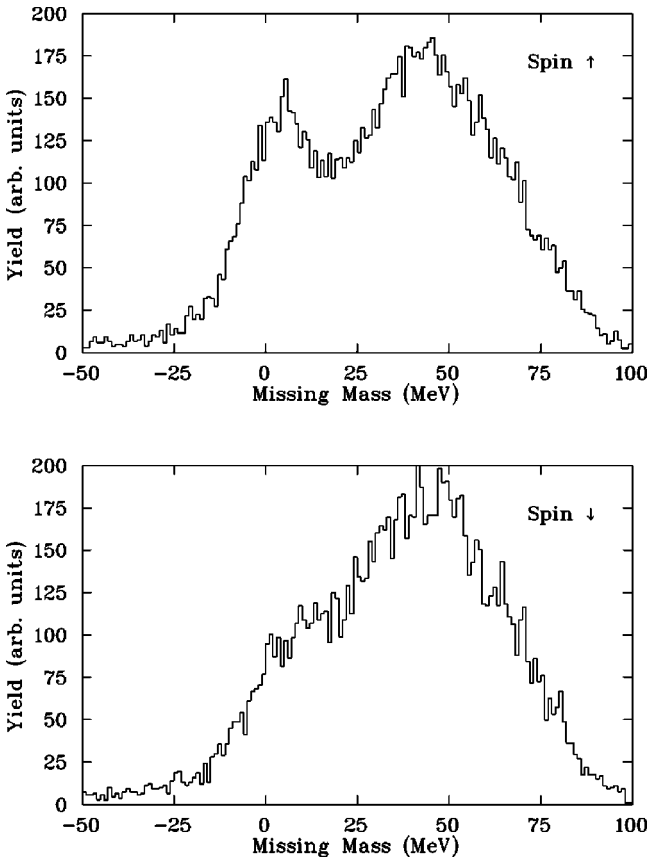

FIG. 4. The π^0 missing mass spectra for spin-up (top) and spin-down (bottom) for the NMS placed at 94°.

an empty glass cell and subtracted from the full-cell data. Because it was not possible to evacuate the ^{3}He target cell for the empty-cell measurements, a cell of very similar diameter and somewhat larger wall thickness (170 μm) was used. Figure 5 shows the π^0 missing mass spectrum from the empty cell target. We fitted a smooth background curve through these data using the equation

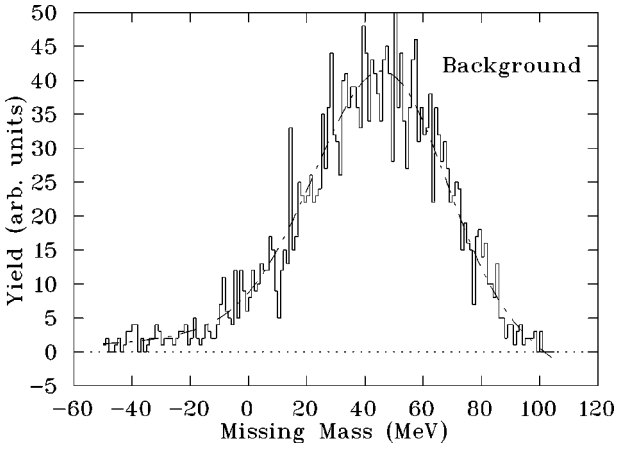

FIG. 5. The π^0 missing mass for the events from the empty glass cell target. The dotted line shows the fit used for background subtraction.

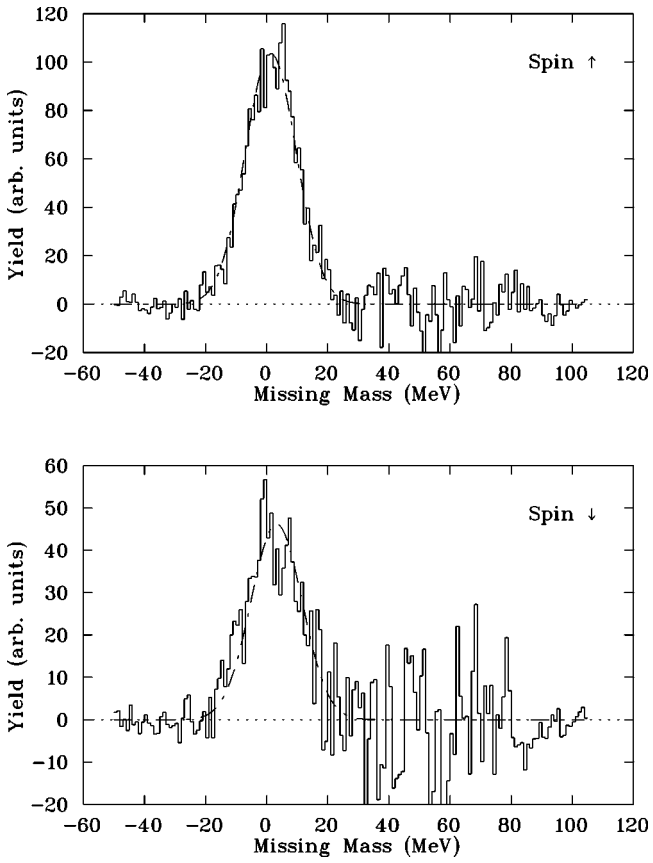

FIG. 6. The π^0 missing mass spectra for spin-up and spin-down after background subtraction, for the NMS placed at 94°.

$$Y_b = a_0 + a_1\mathcal{M} + a_2\mathcal{M}^2 + (b_0 + b_1\mathcal{M})e^{[-c_0(\mathcal{M}-c_1)^2]}, \tag{24}$$

where $\mathcal{M}$ is the missing mass. The value of χ^2 per degree of freedom for the fit was 0.927.

Before subtraction from the full-cell spectra, the yield from the empty target was multiplied by a factor that accounted for the difference in the thickness of the glass walls of the full and empty cells and for the difference in the integrated IC current that was proportional to the integrated beam on target.

Spin-up and spin-down spectra after subtraction of the normalized empty-target spectrum are shown in Fig. 6. For these spectra the NMS was set at 94° on one side of the incident beam and the RTD was set at 40° on the opposite side. Spectra were also taken at one other set of conjugate positions of the NMS and RTD, 75° and 50°, respectively. The two settings covered an angular range for the detected π^0 from 66° to 110° in the center of mass.

F. Monte Carlo simulations

The NMS-RTD detection system was studied by Monte Carlo simulations which were done in two parts. One part simulated the detection of the π^0 through its two-γ decay and included NMS detector geometry, event generation, kinematics, and photon-to-shower conversion and detection. The other part simulated the ^{3}H detection in the recoil triton

detector. It included the detector geometry, the charged particle's energy losses and multiple scattering while passing through the target, air, the wire chamber, and the scintillators. Beam geometry was included also.

The Monte Carlo calculation for the standard NMS setup with the BGO converters and wire chambers gave a solid angle of 6 msr with both the NMS arms and the RTD at a distance of 1 m from the target, when the maximum energy sharing parameter x was chosen to be $x_{\rm cut}=0.4$. The Monte Carlo simulation showed that the RTD was large enough to cover all triton emission angles that are correlated with the π^0's detected in the NMS.

As mentioned above, in the current experiment the acceptance of the NMS was increased (but with loss in energy resolution) by removing the BGO converters and wire chambers so that the opening angles had to be deduced from the locations of the CsI and the energies deposited in the CsI crystals. The Monte Carlo calculations for this configuration and the same $x_{\rm cut}$ and NMS and RTD settings gave an overall acceptance of about 15 msr for detecting a π^0-triton coincidence, an increase by a factor of 2.5 as compared with the standard NMS setup.

IV. THE ASYMMETRIES AND THEIR UNCERTAINTIES

A. Asymmetries

In order to extract the angular distribution of the asymmetries A_y, the angular acceptance of the NMS was divided into four angular bins of size 160 mrad for the NMS set at 94°, and two angular bins of size 240 mrad for the NMS set at 75°. The data analysis techniques were similar to those described in Refs. [4,26]. We used an $x_{\rm cut}$ of 0.6 for the analysis. First, histograms of the appropriate differences and sums of the spin-up and spin-down spectra were created using, for each channel, the equations

$$D=Y_{\uparrow}-\frac{N_{\uparrow}}{N_{\downarrow}}Y_{\downarrow} \tag{25}$$

and

$$S=Y_{\uparrow}+\frac{N_{\uparrow}}{N_{\downarrow}}Y_{\downarrow}-2\frac{N_{\uparrow}}{N_b}RY_b\,. \tag{26}$$

Here $Y_{\uparrow}$ and $Y_{\downarrow}$ are the spin-up and spin-down yields in each angular bin, respectively, and Y_b is the background yield. $N_{\uparrow}$, $N_{\downarrow}$, and N_b are the beam normalization factors for the spin-up, spin-down, and background spectra, Y_b is the yield from the empty target cell, and R is the normalization factor for the background spectrum, which includes the effect of the empty target cell not being identical fo the full target cell. Since the ^{3}He polarization was rotated every 10 min for the A_y measurement, the polarizations for the spin-up and spin-down states were essentially the same, that is, $P_{\uparrow}=P_{\downarrow}=P$ for two adjacent 10-min runs.

The program NEWFIT [27] was used to generate the fits to the histograms D and S, defined in Eqs. (25) and (26), with a Gaussian peak at $\mathcal{M}=0$ MeV. In the fitting of S, the centroid, the width, and the area of the Gaussian were free to vary. The histogram of D was then fitted with a Gaussian peak of the same width and centroid as S.

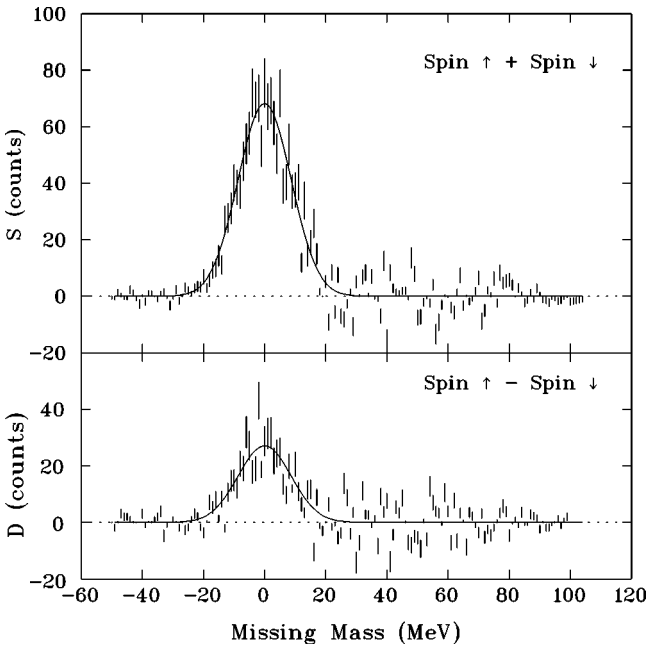

FIG. 7. An example of π^0 missing mass spectra for extracting the yields for S and D at 90°. Top: the normalized summed spectrum after background subtraction; bottom: the difference spectrum. Solid lines: the result of fitting the spectra with NEWFIT [27]. See text.

Figure 7 shows examples of the sum and difference histograms and the fitted peaks that contained the difference and sum yields, Δ and Σ, respectively, for use in the equation for the asymmetry

$$A_y=\frac{(d\sigma/d\Omega)_+-(d\sigma/d\Omega)_-}{(d\sigma/d\Omega)_++(d\sigma/d\Omega)_-}=\frac{1}{P}\frac{\Delta}{\Sigma}. \tag{27}$$

B. Uncertainty of A_y

The uncertainty of A_y [Eq. (27)] is given by

$$\sigma_{A_y}=\frac{1}{P}\frac{\Delta}{\Sigma}\sqrt{\left(\frac{\sigma_P}{P}\right)^2+\left(\frac{\sigma_\Delta}{\Delta}\right)^2+\left(\frac{\sigma_\Sigma}{\Sigma}\right)^2-2\frac{\sigma^2_{\Delta\Sigma}}{\Delta\Sigma}}, \tag{28}$$

where σ_P is the uncertainty in the ^{3}He polarization, which was about $\sim 7\%$. The quantities σ_Δ and σ_Σ are the uncertainties in the integrated yields Δ and Σ. The first term, the standard deviation σ_Δ, was obtained from fitting the difference histogram D. The second term is given by

$$\sigma_\Sigma=\sqrt{\sigma^2_{\Sigma*}+4\left(\frac{N_{\uparrow}}{N_b}Y_b\right)^2\sigma^2_R}, \tag{29}$$

where $\sigma_{\Sigma*}$ is the uncertainty in the integrated yields in the sum spectra before background subtraction. σ_R is the uncertainty in the normalization constant R of the background spectra, which includes the undertainty due to the effect of the empty target cell not being identical to the full target cell.

TABLE I. The measured asymmetries of π^--induced single charge exchange on polarized ^{3}He at 200 MeV.

$\theta_{\rm NMS}$, $\theta_{\rm RTD}$ (deg.)	$\theta_{\rm lab}$ (deg.)	$\theta_{\rm c.m.}$ (deg.)	A_y	ΔA_y
75, 50	60.7	66.3	−0.400	0.137
	74.5	80.6	0.514	0.128
94, 40	76.8	82.9	0.514	0.111
	85.9	92.2	0.983	0.103
	95.1	101.3	0.580	0.107
	104.3	110.3	0.533	0.116

The covariance $\sigma_{\Delta\Sigma}$ is a measure of the correlation between the variables Δ and Σ. It was derived [26] from the standard deviation $\sigma_{Y_\uparrow}$ of the spin-up histogram $Y_\uparrow = 0.5(D + S)$, found after the histogram fitting, the standard deviation σ_Δ, and the standard deviation $\sigma_{\Sigma *}$ by using the relation

$$\sigma^2_{Y_\uparrow} = 0.25(\sigma^2_\Delta + \sigma^2_{\Sigma *} + 2\sigma_{\Delta\Sigma}). \quad (30)$$

.

V. RESULTS AND DISCUSSION

The experimental values of A_y and their uncertainties are given in Table I and are shown in Fig. 8. Also shown in the figures are the results of several theoretical calculations. As expected at far forward angles, all theoretical curves approach the negative of the elementary $p(\pi^-,\pi^0)n$ asymmetry, which is shown by the dotted line. The calculation by Kamalov *et al.* [17], which includes pion rescattering, is shown by the dash-dotted line. This prediction gives negative A_y at all angles and thus misses the large positive A_y measured between 80° and 110°. Another calculation, by Bennhold and Kamalov (private communication, presented in Ref. [30]), includes two-nucleon correlations and yields positive, though too small, A_y in phase with the data between 80° and 120°.

The calculations of Kamalov *et al.* [17] of A_y for elastic scattering from ^{3}He reproduce both the π^+ and π^- data at 100 MeV taken at TRIUMF [2,16]. However, the experimental values for A_y for π^+ scattering obtained at energies across the Δ resonance (142, 180, and 256 MeV) (Refs. [3,4]) could not be reproduced by the conventional DWIA calculations, but they were fitted very well [4] when a Δ-neutron spin-spin interaction was included. Both the latter and the conventional calculations gave too small A_y for π^- elastic scattering at 180 MeV.

The DWIA calculation of the A_y described in this paper and in Ref. [19] qualitatively agrees with the experimental A_y for (π^-,π^0) single charge exchange of this work (Fig. 8). It is also in agreement with the experimental results of π^- elastic scattering on ^{3}He. However, the prediction for π^+ elastic scattering on ^{3}He at 180 MeV does not show the negative A_y near 80° that appear to be characteristic for π^+ scattering at Δ-resonance energies. These results will be presented in a forthcoming paper [31].

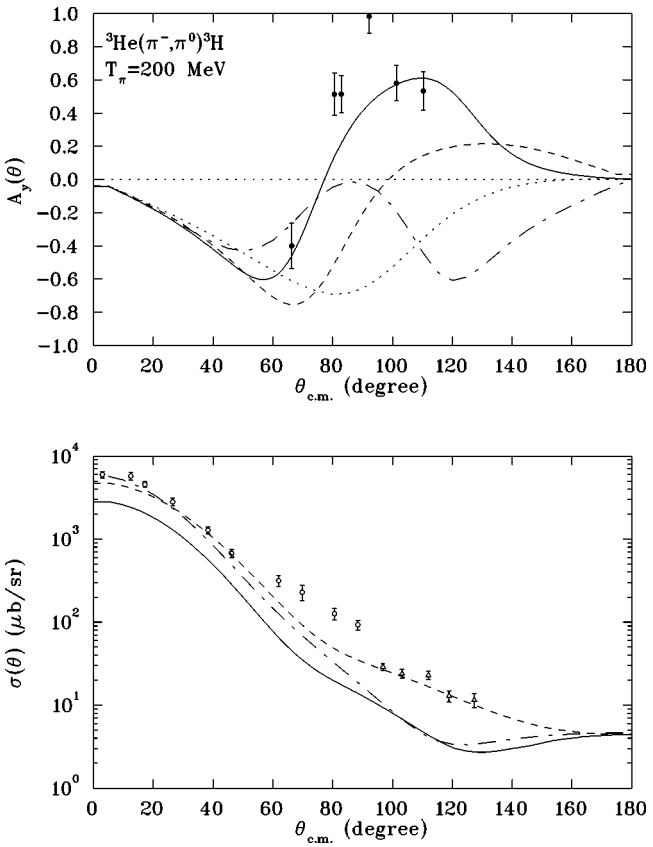

FIG. 8. Angular distributions of A_y (top panel) and differential cross section (bottom panel) for pion charge exchange scattering from polarized ^{3}He at 200 MeV. Experimental data (top panel), this experiment (bottom panel), open triangle, Ref. [25], open circle, Ref. [29]. Solid lines: full-DWIA calculation described in this paper, with $E_{\rm shift}=0$, $X_{at}=0$, and $b_2=(0.0,0.5)$. Dashed lines: same as solid line, half-DWIA calculation. Dash-dotted lines: the prediction of Kamalov *at al.*, including pion rescattering [28]. Dotted line in upper panel: the elementary $p(\pi^-,\pi^0)n$ asymmetry.

We note that the single charge exchange differential cross section (bottom panel in Fig. 8) measured at 200 MeV [24,25,29] were reproduced quite well up to about $\theta_{\rm c.m.} = 70°$ by the DWIA calculations (dashed-dotted lines) of Kamalov *et al.* [17] Our calculations with the half-DWIA, the optical potential multiplied by 1/2 (dashed lines), also reproduced the experimental data quite well, but the full-DWIA calculations (solid lines) are about a factor of 2 too small in absolute cross section at these angles. For a discussion of this point, see Ref. [19].

In an attempt to remove the discrepancies between experimental and theoretical A_y, some of us have considered contributions from the overlaps (SS' and SD) resulting from the small S' and D admixtures to the dominant S part in the wave function of the ^{3}He ground state [31]. It was found that the SS' and SD overlaps do indeed contribute to the spin-dependent amplitude, and particularly that the SD overlap gives an appreciable contribution to the asymmetry at Δ resonance energies for π^+-^{3}He elastic scattering. The DWIA calculation with SD overlap qualitatively agree with A_y of

π^+-^{3}He elastic scattering and are in good agreement with π^--^{3}He elastic scattering. However, the influence of the SD and SS' overlap of A_y on the single charge exchange is so small that it is not readily distinguishable from the result for the dominating π^- single charge exchange with S-state ^{3}He nuclei.

VI. SUMMARY

We have successfully measured asymmetries A_y for π^--induced single charge exchange on polarized ^{3}He, even though the special conditions of this experiment resulted in a π^0 energy resolution of only 20 MeV (FWHM). The use of a triton recoil detector in coincidence with the NMS was essential for separating the recoil ^{3}H from the ^{3}H break-up continuum and from the considerable background from three-body reactions on the nuclei in the glass cell that contained the ^{3}He gas.

The DWIA calculations presented in this paper qualitatively agree with the A_y for single charge exchange but miss the absolute cross section by about a factor of 2 and they do not simultaneously reproduce all elastic asymmetry data satisfactorily. The contributions to the π-^{3}He interaction from the overlaps (SS' and SD) of the S' and D components with the dominant S component in the wave function of the ^{3}He ground state were found to be small for the case of single charge exchange. Previous theoretical analyses of the elastic asymmetries also could not fit all available data. Since the pion-^{3}He system is of great importance to the study of the effective pion-nucleon force in π-nuclear interactions, the data from this work and the earlier data from π^+ and π^- elastic scattering on ^{3}He with polarized and unpolarized targets at several energies are worthy of further analysis.

In principle, cross section and asymmetry data should provide nearly complete information on the spin-independent and spin-dependent amplitudes of π-^{3}He elastic scattering and single charge exchange. In practice, experiments with pion beams on polarized ^{3}He targets are very difficult, so that it has not been possible to take data over a large range of incident energies as would be desirable. Nevertheless, our experiment took the first data for π-induced single charge exchange on polarized ^{3}He. The interpretation of these data as well as the results from the earlier elastic scattering measurements still remains a challenge to theory.

ACKNOWLEDGMENTS

We wish to thank the LAMPF crew for the delivery of a reliable beam. This work was supported in part by the U.S. Department of Energy.

[1] B. Larson, O. Häusser, P. P. J. Delheij, D. M. Whittal, and D. Thiessen, Phys. Rev. A **44**, 3108 (1991).
[2] B. Larson *et al.*, Phys. Rev. Lett. **67**, 3356 (1991).
[3] M. A. Espy *et al.*, Phys. Rev. Lett. **76**, 3667 (1996).
[4] M. A. Espy *et al.*, Phys. Rev. C **56**, 2607 (1997).
[5] R. Tacik *et al.*, Phys. Rev. Lett. **63**, 1784 (1989).
[6] R. Meier *et al.*, Phys. Rev. C **42**, 2222 (1990).
[7] Yi-Fen Yen *et al.*, Phys. Rev. Lett. **66**, 1959 (1991).
[8] Yi-Fen Yen, Ph.D. thesis, University of Minnesota, 1991.
[9] Yi-Fen Yen *et al.*, Phys. Rev. C **50**, 897 (1994).
[10] J. T. Brack *et al.*, Phys. Rev. C **45**, 698 (1992).
[11] R. Mach and S. S. Kamalov, Nucl. Phys. **A511**, 601 (1990).
[12] P. B. Siegel and W. R. Gibbs, Phys. Rev. C **48**, 1939 (1993).
[13] R. A. Brandenburg, Y. E. Kim, and A. Tubis, Phys. Rev. C **12**, 1368 (1975).
[14] J. L. Friar, B. F. Gibson, G. L. Payne, and C. R. Chen, Phys. Rev. C **34**, 1463 (1986).
[15] D. R. Tilly, H. R. Weller, and H. H. Hasan, Nucl. Phys. **A474**, 2 (1987).
[16] B. Larson *et al.*, Phys. Rev. C **49**, 2045 (1994).
[17] S. S. Kamalov, L. Tiator, and C. Bennhold, Few-Body Syst. **10**, 143 (1991).
[18] C. Bennhold, B. K. Jennings, L. Tiator, and S. S. Kamalov, Nucl. Phys. **A540**, 621 (1992).
[19] W. R. Gibbs and B. F. Gibson, Phys. Rev. C **43**, 1012 (1991).
[20] W. B. Kaufman and W. R. Gibbs, Phys. Rev. C **28**, 1286 (1983).
[21] P. B. Siegel and W. R. Gibbs, Phys. Rev. C **48**, 1939 (1993).
[22] W. J. Cummings, O. Häusser, W. Lorenzon, D. R. Swenson, and B. Larson, Phys. Rev. A **51**, 4842 (1995).
[23] NMS-Collaboration, Proposal For A High Resolution Spectrometer For Neutral Mesons, Los Alamos National Laboratory, 1989.
[24] J. D. Bowman, Nucl. Phys. **A335**, 375 (1980).
[25] J. Käellne *et al.*, Phys. Rev. Lett. **42**, 159 (1979).
[26] J. M. O'Donnell (unpublished).
[27] C. L. Morris, program NEWFIT (private communication).
[28] S. S. Kamalov, L. Tiator, and C. Bennhold, Phys. Rev. C **47**, 941 (1993).
[29] M. D. Cooper *et al.*, Phys. Rev. C **25**, 438 (1982).
[30] D. Dehnhard, Acta Phys. Pol. B **27**, 3019 (1996).
[31] Q. Zhao and W. R. Gibbs (unpublished).